Variations in F and Cl contents in apatites from magnetite–apatite ores in northern Chile, and their ore-genetic implications

PETER J. TRELOAR

School of Geological Sciences, Kingston University, Penrhyn Road, Kingston-upon-Thames, Surrey KT1 2EE, UK

AND

HOWARD COLLEY

School of Construction and Earth Sciences, Oxford Brookes University, Gypsy Lane, Oxford OX3 0BP, UK

Abstract

Magnetite–apatite deposits associated with the Atacama Fault Zone of northern Chile are interpreted here, on field criteria, as being the products either of hydrothermal fluids with a strong magmatic signature, or of late-stage Fe-rich magmas mixed with an aqueous fluid. Even in the Chilean iron belt, apatite-rich magnetite deposits are a rarity. Variations in F- and Cl- contents in apatites, strongly zoned with respect to halogens, are indicative of primary variations in f_{HF} and f_{HCl} in the hydrothermal fluids. Small variations in halogen fugacities in the aqueous fluid are capable of buffering large variations in halogen content within apatite crystals in equilibrium with that fluid. The recorded halogen zonation profiles are inconsistent with crystallization of the apatites simply from a volatile-rich, late-stage fractionation Fe-rich magma, or its derived magmatic vapour. It is more likely that they are the result of mineral–fluid buffering with a fluid that represents the mixing of a magmatically-derived aqueous fluid with a meteoric fluid that has variably scavenged Ca and Cl from within the country rocks. The source magma of the former is probably an Fe-P enriched acidic magma, derived by fractionation of primary calc-alkaline basic magmas.

KEYWORDS: Apatites, Chile, ore-genesis, halogen.

Introduction

MAGNETITE-RICH bodies, with or without apatite, are characteristic of the westernmost part of the Chilean ore province (Clark *et al.*, 1976; Sillitoe, 1976; Frutos, 1982; Boric *et al.*, 1991; Nystrom and Henriquez, 1994), and, indeed, of much of the Circum-Pacific region (Park, 1972). The genesis of such deposits is, however, poorly understood. They are considered by some to represent deposits directly crystallized from an iron-rich 'magma', either intrusive in nature, as at Kiruna in Sweden (Geijer, 1960; Frietsch, 1978), or extrusive, as at El Laco in Chile (Park, 1961, Nystrom and Henriquez, 1994) or Pleito-Melon in Chile (Travisany *et al.*, 1995). A number of alternative genetic processes have, though, been suggested for such deposits (c.f. Romer *et al.*, 1994). For instance, Parak (1975, 1984) re-interpreted the Kiruna ores as being exhalative-sedimentary in origin. Cliff *et al.* (1990) and Blake (1994) have argued for the role of a high-temperature hydrothermal fluid in their formation. Oreskes *et al.* (1994) cite fluid inclusion and oxygen isotope data, together with a widespread argillic alteration, to argue that significant proportions of the El Laco deposit may have formed from moderate-temperature, vapour-rich near-surface hydrothermal fluids. Bookstrom (1977) described the El Romeral deposit in Chile as having a hydrothermal origin and similar conclusions have been reached for magnetite-rich deposits from the Arequipa segment of the Peruvian Coastal batholith by Atkin *et al.* (1985) and Vidal

Mineralogical Magazine, April 1996, Vol. 60, pp. 285–301

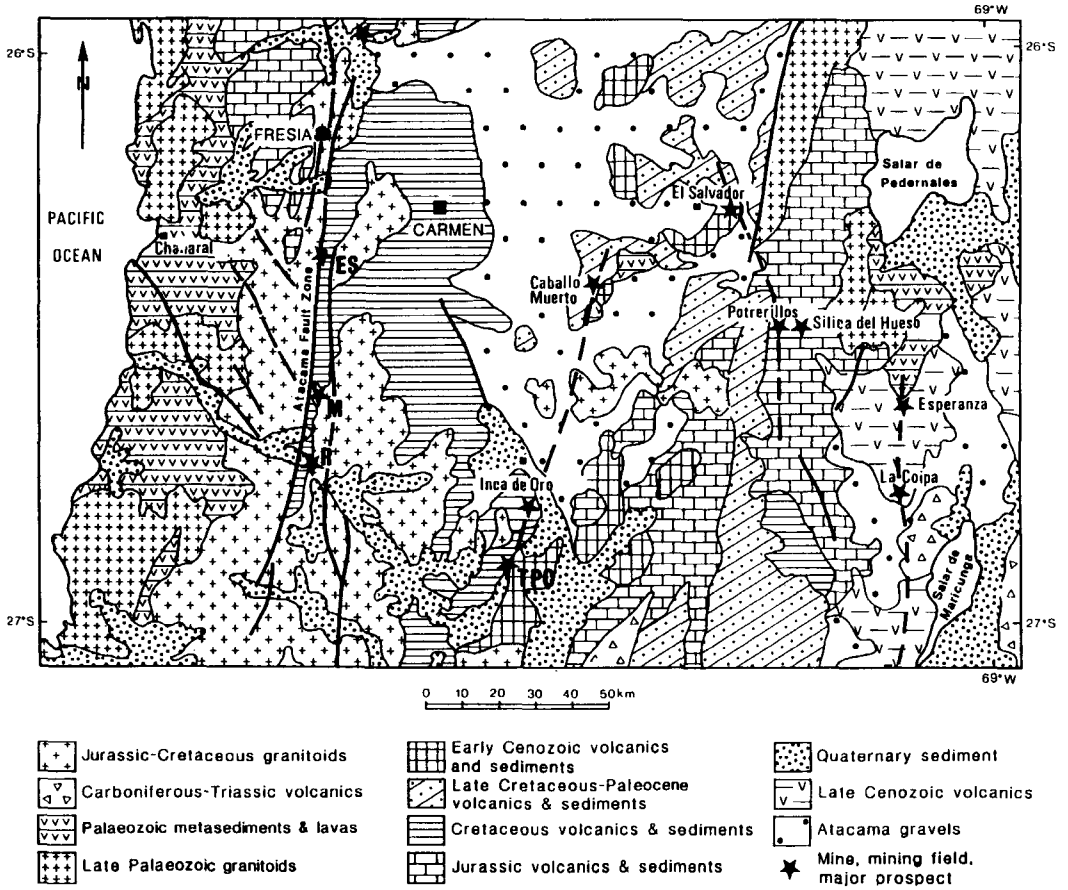

FIG. 1. Geological map of part of northern Chile showing the location of the Fresia and Carmen deposits and their spatial relationship to both the Atacama fault system and the Jurassic-Cretaceous magmatic arc. Other mines: M: Mantoverdi. R: Rosario. ES: El Salado. TPC: Tres Puntas-Chimberos mining field.

(1985). As an extreme view, based on studies of the Olympic Dam deposit, Hitzman *et al.*, (1992) infer that purely magmatic processes are unlikely to account for the evolution of any magnetite–apatite deposit.

The origin of magnetite–apatite deposits is thus clearly enigmatic. Their common occurrence and widespread distribution within the circum-Pacific region implies that their genesis is linked to continent-margin, subduction-related magmatic processes. The north Chilean part of the Andean coastal batholith apparently includes both magmatic (El Laco) and hydrothermal (El Romeral) magnetite-rich deposits. Thus, the magmatic and hydrothermal deposits probably represent different stages in the continuum that spans the transition from late-stage, volatile-rich, iron-enriched magmas to their evolved hydrothermal fluids. This view is similar to that of Park (1972) who, reviewing Pacific Basin iron deposits, envisaged a spectrum of deposits ranging from magnetite flows to watery, iron-rich pegmatites. It is also similar to that of Henriquez *et al.* (1994), who argued that the Chilean magnetite-apatite deposits all have a common magmatic origin, and that they formed during the evolution of an ore magma that passed through intrusive or extrusive, to pegmatitic to hydrothermal stages.

Some deeply mined, magnetite–apatite deposits from within, and to the east, of the Atacama Fault Zone of northern Chile present the opportunity for the potential derivation of solutions to the problems of the genesis of such deposits. In this study halogen

chemistries in apatites are used in order to derive answers to three main questions. What controls total apatite concentration in the rock? Why do only some magnetite-rich deposits in the region contain apatite? What is the relationship between magmatic and hydrothermal processes in their genesis?

Geological setting of the magnetite-apatite deposits

A number of primary iron-oxide deposits occurs within, or close to, the Atacama Fault Zone in the El Salado area of northern Chile (Fig. 1). These include the iron-apatite ores discussed in this paper, magnetite-hematite ores without apatite, and specular hematite ores commonly associated with copper sulphide mineralization. The majority of deposits occur within the Lower Cretaceous Los Cerros Florida formation, usually where the formation is intruded by members of the Sierra Pastenes batholith.

Los Cerros Florida formation

This is predominantly composed of plagiophyric, porphyritic andesitic rocks that occur as massive to poorly bedded breccias and lavas. There are minor intercalations of recrystallized limestone and sandstones, particularly towards the base of the formation. A pervasive low-grade metamorphism is characterized by development of abundant chlorite and subsidiary epidote, sericite, fibrous amphibole and iron oxides. Naranjo (1978) considered the sedimentary sequence to be of continental origin with rare marine incursions. The Jurassic to Early Cretaceous basic volcanic rocks of northern Chile are generally high-K calc-alkaline rocks with P_2O_5 contents of generally between 0.30 and 0.50% (Buchelt and Cancino, 1988; Levi *et al.*, 1982; Pichowiak, 1993; Rogers and Hawkesworth, 1989). Basalts and andesites are frequently spilitic with Na_2O contents of up to ~6 wt.% (Levi *et al.*, 1982).

Sierra Pastenes batholith

This is principally composed of tonalitic intrusions with smaller bodies of granodiorite, quartz monzonite, diorite and gabbro. Plagioclase (An_{10-50}) and quartz dominate in the tonalites along with minor amounts of Fe-rich biotite and amphibole. Apatite inclusions are common in the amphibole. The more mafic members of the suite contain abundant plagioclase (An_{30-50}) with ortho- and clinopyroxene. The elongate shapes of the intrusive bodies, and the presence of mylonitic and cataclastic zones along the pluton margins, are consistent with suggestions that granite emplacement has been controlled by movements within the Atacama Fault Zone (Grocott *et al.*, 1994). The Rb-Sr whole rock and U-Pb zircon data constrain an emplacement age of between 125 and 130 Ma (Berg and Baumann, 1985). The Sr and Nd isotope data and whole rock chemistry (Table 1) are indicative of melting of a mantle I-type source above a subduction zone, with little crustal contamination (Berg and Baumann, 1985; Brook *et al.*, 1987; Brown, 1988).

TABLE 1. Geochemistry (major elements and selected trace elements) of granodiorites of the Sierra Pastenes batholith. These data, provided by M. Brown, are unpublished XRF results from the University of Keele

Sample	S1006	S1007	S1008
SiO_2	62.05	61.65	57.01
TiO_2	0.75	0.98	1.55
Al_2O_3	16.62	15.92	16.29
$Fe_2O_3^t$	6.15	6.70	4.47
MnO	0.10	0.10	0.15
MgO	2.45	2.47	4.69
CaO	5.14	4.95	12.22
Na_2O	4.19	3.96	4.02
K_2O	2.26	2.48	0.20
P_2O_5	0.18	0.24	0.02
LOI	0.58	0.52	0.40
Total	100.47	99.97	101.02
Rb	54	55	<2
Sr	363	347	544
Y	27	31	27
Zr	132	189	109
Nb	6	7	6
Th	2	5	<1
Ba	398	449	109
La	19	26	2
Ce	42	54	24
Nd	6	39	22
Cl	1442	1602	933
S	142	137	119

Atacama Fault Zone

This is a trench-parallel, strike-slip fault system (Brown *et al.*, 1993) that runs N–S through northern Chile for over 1000 km. Although displacement during the Mesozoic has been described as dominantly left-lateral (Scheuber and Andriessen 1990), the fault zone had a complicated movement history. Within the El Salado sector, between 26 and 27°S, two distinct displacement trajectories are determined for the Jurassic and Cretaceous. An

early phase of ductile dip-slip movement with E-side down (Colley *et al.*, 1989), was succeeded by sinistral, strike-slip movement which commenced within the ductile field but continued, throughout a falling temperature regime, into the brittle field (Brown *et al.*, 1993). Shearing was synchronous with granite emplacement (Grocott *et al.*, 1994). The later, brittle, stages of the left-lateral strike-slip movement postdate granite emplacement, and were accompanied by widespread iron mineralization. Brittle faults are coated with magnetite, large areas of weakly fractured basic igneous rocks are iron stained on their surfaces, and large, subeconomic, Fe and Fe-Cu deposits located within dilational fault jogs, such as the Mantoverdi mine, are currently being evaluated and/or exploited. In a small number of deposits, magnetite, which is the dominant mineral within this part of the fault system, occurs in association with apatite and amphibole.

Geology and mineralogy of the magnetite–apatite deposits

The Fresia deposit is a magnetite–apatite deposit located within the Atacama fault system, north of El Salado (Fig. 1). The deposit is hosted by massive, andesitic rocks of the Los Cerros Florida Formation which form a series of thick lava flows cut by andesitic dykes that range from microgabbro to microdiorite. The rocks show a sub-ophitic texture with well-zoned, flow-aligned plagioclase phenocrysts in a pyroxene matrix. Both flows and dykes are strongly altered. The deposit is an elongate, steep-sided, sheet-like body <20 m wide. It has a sinuous shape, controlled by two sets of faults trending at 080° and 065°. Slickensides, developed on both fault sets, are shallow plunging. The fault geometry is typical of pull-apart zones or dilational jogs developed within strike-slip systems (Sibson, 1977), and is interpreted as being indicative of localized dilation within the N-S trending Atacama fault system.

Carmen Mine lies some 20 km E of the Atacama fault system (Fig. 1) within porphyritic andesites of the Los Cerros Florida formation. The shape of the open pit (400 m long and 150 m wide, with the long axis trending NE–SW) is a function of the intersection of an E-W trending set of steep faults with subhorizontal slickensides, and a N-trending array of conjugate dip slip faults. Both the shape of the body, and the geometry of the controlling faults, are consistent with localized dilation. The N-trending fault array constrains the ore distribution which is characterized by N-trending bands of Fe-rich ore up to 20 m in width. To the north and south of the body, country rocks are iron-stained along parallel N-trending zones.

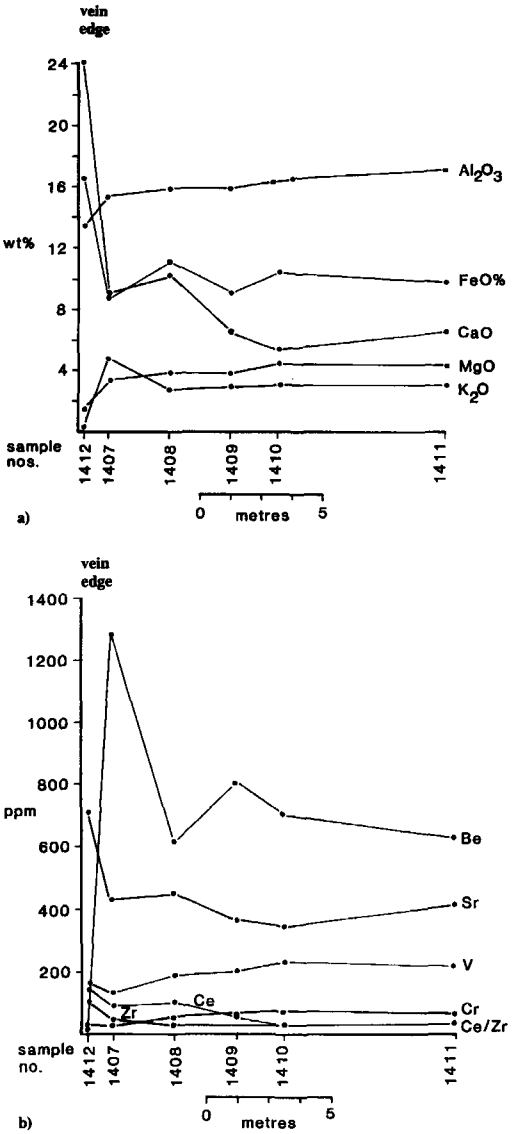

FIG. 2. Geochemical profiles across the altered wall rock to the Fresia deposit. (*a*) Selected major elements, (*b*) selected trace elements.

Wallrock alteration

In the vicinity of the deposits the country rocks have undergone an intense propylitic alteration with widespread growth of epidote, together with chlorite, calcite and a calcic amphibole from the tremolite–actinolite solid-solution series. Plagioclase (An_{40}) is

replaced by epidote and mafic minerals are pseudomorphed by chlorite, serpentinite and iron oxides. Epidote is commonly the dominant alteration mineral although actinolite is dominant in some samples. The country rocks have been brecciated along the margins to the deposits, with the voids infilled by magnetite together with fibrous apatite and actinolite.

The visible alteration halo to the larger veins extends for some 5 m. At Fresia, the edge of the main magnetite-apatite ore vein is marked by strongly sheared epidote-rich rock. This passes outwards into propylitized microgabbro, with epidote veinlets extending for some 7 m beyond the main vein. Figure 2 shows the extent of geochemical changes that accompanied wallrock alteration from the epidote-rich rock (sample 1412) on the edge of the main Fresia vein outward to unaltered microgabbro (sample 1411). The other samples in the traverse show alteration but no obvious veining by either magnetite or apatite. The chemical effects of the hydrothermal alteration are shown most markedly by Ba, Sr, CaO, K_2O and FeO. Given that FeO will relate to iron-rich fluids and the other elements are major or trace components of apatite, or products of feldspar destruction, these trends are to be expected.

Ore textures

The Fresia and Carmen deposits are characterized by epigenetic, massive iron ore bodies, which are dominantly magnetite although with local hematite patches. The ore bodies range in size from large subvertical sheets up to 20 m in width down to veinlets no more than a few mm in width. Apatite commonly occurs as individual coarse crystals 'floating' within a matrix of magnetite (Fig. 3*a*), although its distribution throughout the magnetite ore is non-uniform. Some of the apatite crystals are of spectacular size, attaining lengths of up to about 50 cm long, and zoned with rose pink cores grading to white rims. Large ragged apatites contain inclusions of actinolite and magnetite, but are frequently fractured, with fractures infilled by very narrow veinlets of magnetite (Fig. 3*b*) and epidote.

In addition to coarse crystals floating within the main magnetite ore, apatite also occurs within planar zones contained within, apparently homogeneous, magnetite zones (Fig. 3*a*). Often these apatites show a 'comb'-like texture, having grown as delicate acicular crystals with a strongly preferred orientation perpendicular to the vein wall. In this case, the pattern is similar to that of fibrous crystals growing into an opening hydrothermal fracture (Ramsay and Huber, 1983). Both apatite and amphibole apparently nucleated on an iron-rich substrate that forms the zone, or vein, wall and grew inwards into the zone perpendicular to its margins. While both apatite and amphibole grew perpendicular to block faces and vein walls at the vein margins, they are randomly oriented within the centres of such veins. Similar features are also seen along the margins of the orebodies. At Carmen the country rock has clearly been brecciated. Each breccia fragment has a selvedge of magnetite on which needles and blades of apatite and amphibole have nucleated, and grown outward from the breccia fragment, perpendicular to its surface, into the surrounding magnetite ore (Fig. 3*c*). Similar textures have also been described from Kiruna (Cliff *et al.*, 1990). Many of the apatite crystals have fibrous margins, and some have been completely replaced by fibrous aggregates of fine-grained apatite reflecting a late-stage hydrothermal alteration process.

Some mm- to cm-wide fractures within the altered country rock, are infilled with magnetite or magnetite and apatite (Fig. 3*d*). Occasionally, such fractures have margins of magnetite and crystalline epidote, fibrous apatite and calcite in their centres. Within both ore bodies and adjacent country rocks, the main assemblages are cut by late-stage epidote and calcite filled veins and, at Carmen only, by gypsum veins. At Fresia Mine, both apatite and magnetite are cut by such veins, although at Carmen, only the magnetite appears to be so affected. In places these epidote-filled veins are themselves cut by fine magnetite veinlets.

A generalized paragenetic sequence is summarized in Table 2. Overall, the textures are characteristic of hydrothermal, or magmatic, brecciation of country rock sequences, with fractures and brecciated voids having been infilled by hydrothermally-deposited material, in this case the magnetite ore. As they always nucleate on a magnetite layer, growth of apatite and amphibole must have postdated the earliest precipitation of Fe-ore. Apatite, amphibole, epidote and magnetite must all have formed a stable paragenetic assemblage within the hydrothermal environment over a period of time. Multiple phases of magnetite growth, with or without apatite, are evident. Similar textures have been described from Kiruna (Frietsch, 1978; Cliff *et al.*, 1990). The infilling of late-stage fractures within apatite by magnetite implies that, towards the end of the mineralization period, apatite was no longer stable. Three main factors suggest that evolution of the magnetite–apatite deposits was influenced by hydrothermal processes located within an active fault system: the localization of iron mineralization onto brittle fault planes; the widespread hydrothermal iron mineralization and extensive propylitic alteration that are developed throughout the zone; and the intense greenschist-facies wallrock alteration associated with the deposits.


0
5
10
CENTIMETRES
a)

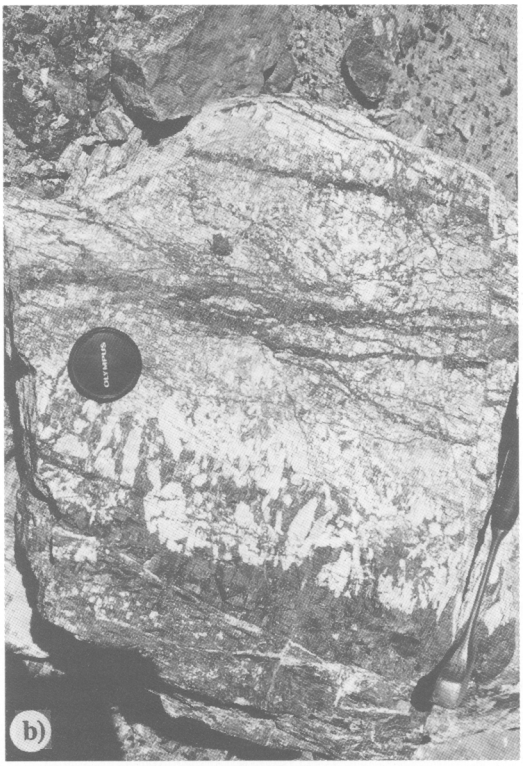
b)


c)

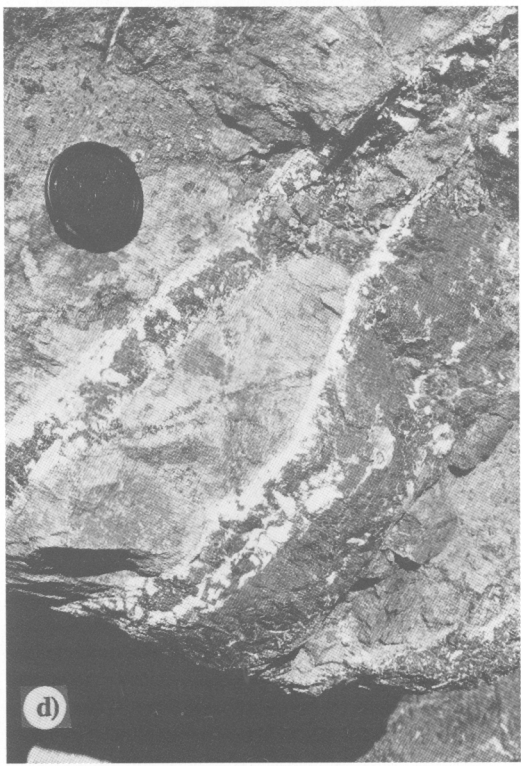
d)

TABLE 2. A generalized sequence of paragenetic events for the Fresia and Carmen apatite-magnetite deposits

1. Propylitic alteration of host-rock with prominent development of epidote, minor silicification and hematization.
2. Brecciation of the country rock and deposition of magnetite-rich, apatite-poor ore with continuing epidotization; a magnetite-rich 'skin' forms around breccia clasts.
3. Growth of apatite and actinolite on the edges of breccia clasts and veins with the development of a comb-layering.
4. Development of substantial voids and growth of giant apatites, up to 50 cm in length, containing inclusions of magnetite and actinolite.
5. Infill of void by magnetite-rich ore.
6. Fracturing of previously formed ore and infill by narrow veinlets of coarsely crystalline magnetite, specularite and epidote.
7. Late growth of gypsum in remaining voids (Carmen only).

Mineral chemistry

The apatite–magnetite ores are dominated by magnetite, apatite and amphibole. The iron ore phase is dominantly magnetite although all gradations towards haematite can be recognized. Maximum contents of minor and trace elements include 1.21% TiO_2, 0.75% Al_2O_3, 0.20% MnO and <1.0% MgO.

Electron microprobe analysis shows primary apatites (Table 3) to be chlorine and fluorine bearing, with up to 6.82% Cl and 2.87% F. The former represents 100% of the end-member chlor-apatite and the latter 75% of the end-member fluor-apatite. Most apatites are strongly zoned with respect to Cl and F, which are negatively correlated. Although both Cl and F contents can be derived directly from microprobe data, carbonate and hydroxyl components cannot. Carbonate is not an important phase in the altered, wall rock envelopes to the deposits. What carbonate we have identified is restricted to narrow, late-stage veins. Hence, we make the assumption that CO_2 was a minor component of the ore forming fluid and that the carbonate-apatite end member is, at most, a minor component of the apatites. On this basis, the value of $X_{OH\text{-}ap}$ has been calculated by difference such that $X_{F\text{-}ap} + X_{Cl\text{-}ap} + X_{OH\text{-}ap} = 1$. The analysed apatites show extensive solid solution between the hydroxy-apatite (OH-ap), fluor-apatite (F-ap) and chlor-apatite (Cl-ap) end-members.

Detailed microprobe traverses (Table 3, Fig. 4) were made across apatites from three samples. Sample 1134, from Carmen mine, has high values of $X_{F\text{-}ap}$ for most of the traverse but with a decrease in $X_{F\text{-}ap}$ and increase in $X_{Cl\text{-}ap}$ and $X_{OH\text{-}ap}$ near to the rim (Fig. 4*a*). Sample 1531 is from a planar zone within the Fresia ore body into which acicular apatite and amphibole crystals grew inward from the zone edge. Apatites from the zone margin, which grow perpendicular to the zone wall, are inferred as having grown during opening of the zone. These have $X_{Cl\text{-}ap}/X_{F\text{-}ap}$ ratios that increase from core towards the rim from 0.485 in their cores to c. 25 near the rims (Table 3, Fig. 4*b*). By contrast, apatites within the zone centre have $X_{Cl\text{-}ap}/X_{F\text{-}ap}$ ratios of *c.* 28 in their cores decreasing to 0.87 in the near rim regions before increasing again to *c.* 16 right at the rim. In this sample, apatites from both marginal and central parts of the zone show increases in $X_{OH\text{-}ap}$ in the extreme rim regions (Table 3, Fig. 4*c*). Apatites from sample 1528, also from the Fresia body, show an increase in $X_{F\text{-}ap}$ from the core towards the rim, although with a decrease in $X_{F\text{-}ap}$ and increase in both $X_{Cl\text{-}ap}$ and $X_{OH\text{-}ap}$ in the extreme rim regions (Table 3). Cl-maps and traverses across this sample

FIG. 3. Field photographs of the magnetite-apatite deposits showing some important textural relationships. (*a*) Magnetite ore from the Fresia deposit with both isolated ovoid apatite crystals, and a zoned band of apatite within which many of the apatite crystals have grown at a high angle to the band margins. (*b*) Fine magnetite-rich veinlets filling fractures within apatites from the Carmen deposit. (*c*) Brecciated and altered country rock from the margin of the Carmen deposit. The country rock blocks are epidotized. They are rimmed by a thin skin of magnetite outward from which, into the magnetite ore, grow acicular amphibole and apatite crystals. (*d*) Magnetite–apatite veins in propylitised altered country rock.

TABLE 3. Phase chemistries of apatites from three magnetite-apatite bearing ore samples. Mineral formulae calculated on the basis of 12.5 oxygens. n rim: near rim. Analyses carried out on the Microscan Mk 9 wavelength dispersive electron microprobe housed in the Dept of Earth Sciences, Oxford University. F analyses were obtained using a W/Si 60A multilayer pseudocrystal (Potts and Tindle, 1989) with counts processed through a flow counter fitted with a thin mylar window

	1531 Edge of zone			1531 Inner part of zone		
	core	n rim	rim	core	n rim	rim
CaO	56.09	52.06	52.56	52.74	54.31	53.18
FeO	0.10	0.12	0.98	0.37	0.07	1.21
P_2O_5	41.09	40.09	38.39	40.20	41.09	38.93
Cl	1.92	5.87	3.65	6.33	2.73	3.95
F	2.12	0.13	0.13	0.12	1.65	0.13
-O (= F+Cl)	1.33	1.38	0.88	1.48	1.31	0.95
Tot	99.99	96.89	94.82	98.28	98.52	96.45
Y_2O_3	0.04	0.03	0.06	0.07	0.02	0.07
La_2O_3	bd	bd	bd	bd	bd	bd
Ce_2O_3	0.04	0.01	0.05	0.05	0.01	0.01
Pr_2O_3	bd	0.01	0.01	bd	bd	bd
Nd_2O_3	0.02	0.22	0.13	0.07	0.12	bd
Sm_2O_3	0.06	bd	0.11	0.01	0.17	0.02
Ca	5.138	4.970	5.168	4.890	5.038	5.146
Fe	0.007	0.002	0.014	0.052	0.001	0.017
P	2.973	3.024	2.982	2.945	3.012	2.977
Cl	0.278	0.886	0.567	0.928	0.401	0.605
F	0.573	0.036	0.038	0.033	0.452	0.037
OH = 1–F–Cl	0.149	0.078	0.395	0.039	0.147	0.358

	1528				1134			
	core	n rim	n rim	rim	core	core	n rim	rim
CaO	51.57	53.89	52.15	52.81	55.46	54.83	55.67	55.24
FeO	0.06	0.07	0.37	1.31	0.03	0.03	0.02	0.06
P_2O_5	39.25	40.15	40.58	39.25	40.96	40.37	41.05	40.31
Cl	6.59	1.90	2.67	3.67	0.19	0.15	0.34	2.30
F	0.32	1.31	0.88	0.28	2.87	2.83	2.51	0.63
-O = (F+Cl)	1.62	0.98	0.97	0.95	1.25	1.23	1.13	0.78
Tot	96.17	96.34	95.68	96.37	98.26	96.98	98.46	97.76
Y_2O_3	0.22	0.18	bd	bd	bd	0.17	bd	bd
La_2O_3	0.23	0.06	0.15	0.04	0.01	0.02	0.01	0.01
Ce_2O_3	0.56	0.37	0.54	0.12	0.17	0.18	0.20	0.13
Pr_2O_3	0.09	0.02	bd	bd	0.02	0.07	0.05	bd
Nd_2O_3	0.43	0.34	0.28	0.22	0.19	0.26	0.08	0.24
Sm_2O_3	0.03	0.06	0.16	0.17	0.07	0.10	0.02	0.07
Ca	4.973	5.125	4.985	5.136	5.121	5.132	5.143	5.216
Fe	0.004	0.005	0.027	0.104	0.002	0.002	0.001	0.004
P	2.990	3.017	3.065	3.016	2.989	2.986	2.996	3.008
Cl	1.005	0.286	0.404	0.564	0.028	0.022	0.050	0.344
F	0.091	0.368	0.248	0.080	0.783	0.782	0.684	0.176
OH = 1–F–Cl	0.000	0.346	0.348	0.356	0.189	0.196	0.266	0.480

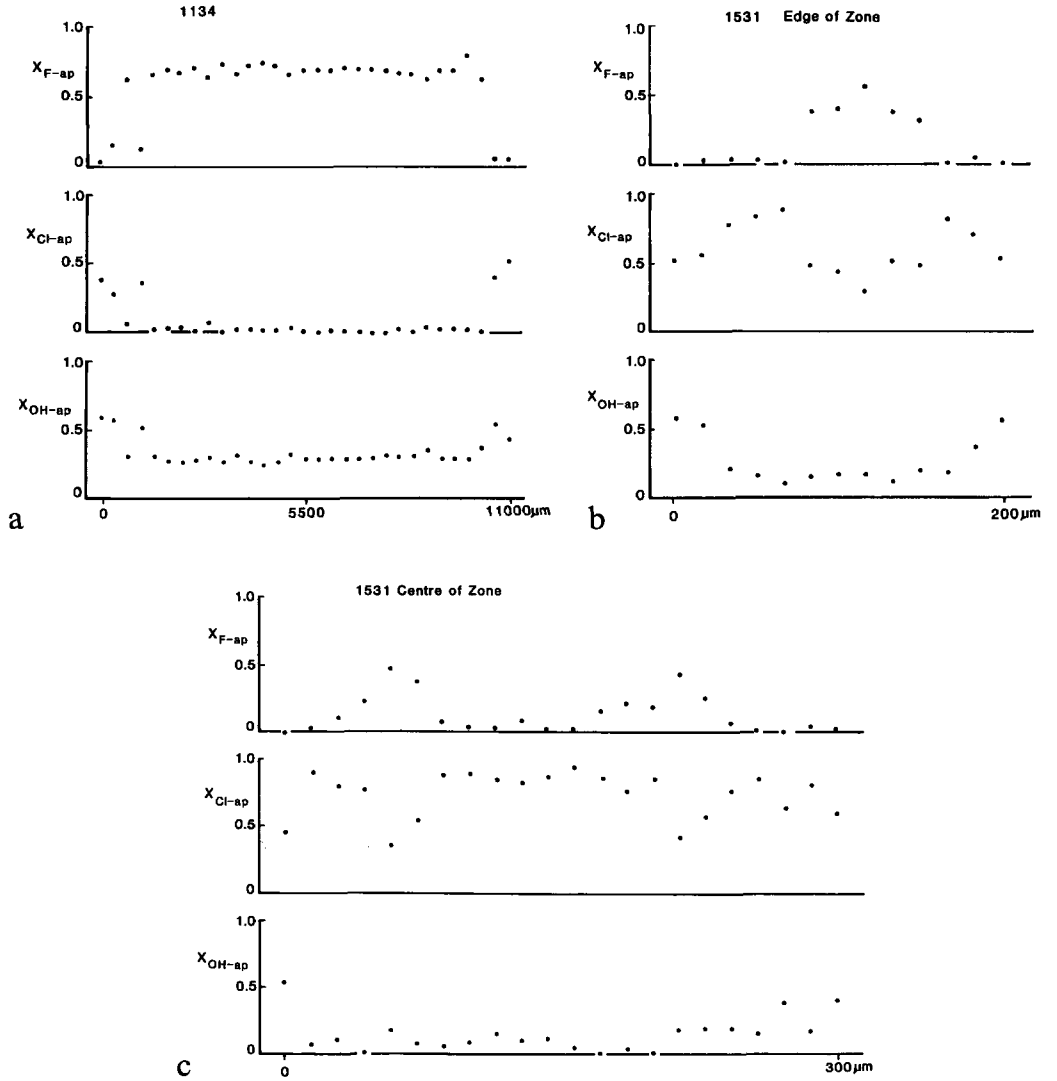

FIG. 4. Compositional profiles across zoned apatite crystals. The profiles are based on analysed F and Cl contents with OH content calculated on the basis: $X_{F\text{-}ap} + X_{Cl\text{-}ap} + X_{OH\text{-}ap} = 1$. (*a*) Sample 1134 from the Carmen deposit, (*b*) sample from the vein margin of sample 1531 from the Fresia deposit, (*c*) sample from the vein centre of sample 1531.

show the strong Cl zonation (Fig. 5*a,b*). Some of the apatites are also zoned with respect to the *REE*. In sample 1528, the light *REE* Ce, La and Nd are enriched in cores with respect to rims (Fig. 5*c*). The apatite from the Carmen deposit analysed here (sample 1134) is much richer in F than those analysed from the Fresia deposit. Apatites in the Kiruna deposits also have high F contents (Frietsch, 1978; Cliff *et al.*, 1990). This has been cited by Frietsch (1978) as indicative of a magmatic origin for the Kiruna deposits. If high F contents in apatites are truly indicative of an igneous origin, then this might imply that the Carmen deposit is of igneous origin or, if influenced by hydrothermal processes, has seen a lesser amount of mixing with hydrothermal fluids than the Fresia deposit.

Amphiboles are members of the tremolite-actinolite solid solution series (Fig. 6*a*), with X_{Fe} values ranging from 0.11 to 0.49. The Al_2O_3 contents are as high as 3.6%, although they are usually <2.5%. The

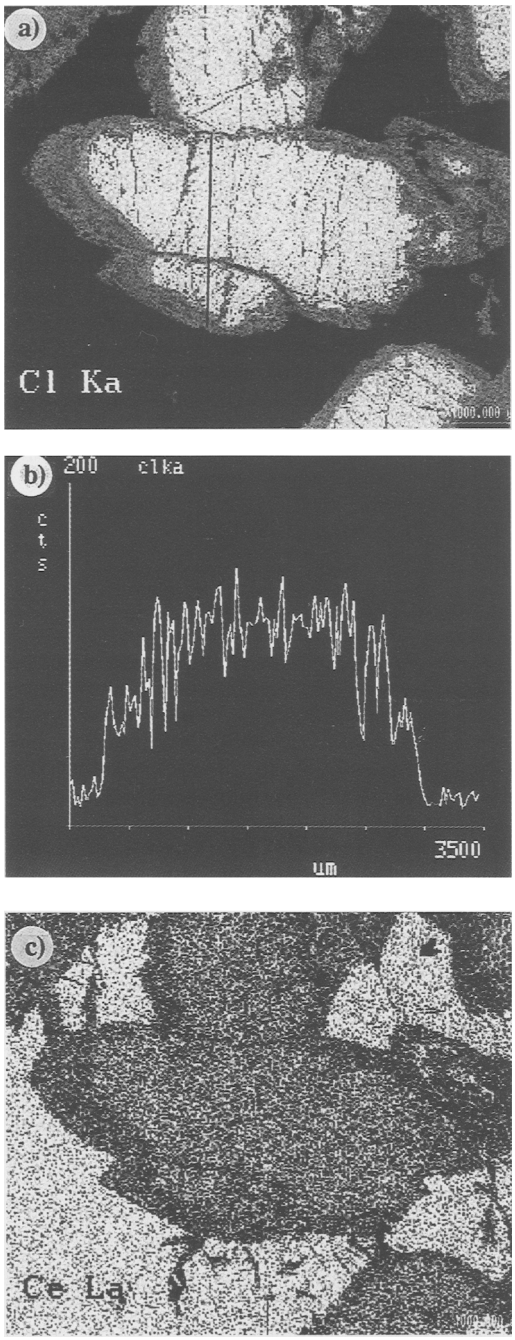

FIG. 5. Chemical zonation in an apatite from the Fresia deposit, sample 1528. (*a*) Cl-map showing enriched Cl contents in the core. Scale bar: 1000 μm. (*b*) Cl-traverse across along the traverse line across the grain shown in Fig. 5*a*. (*c*) Ce-map showing enriched Ce, and hence *LREE*, contents in the apatite core.

Na_2O and K_2O contents are low, with total alkali content always <0.50%. Thus the amphiboles show limited edenitic and pargasitic substitutions (Fig. 6*b*). There is no significant compositional difference between amphiboles in the wall rocks, and those within the ore bodies. The Cl-contents are always <0.25 wt.%. The F levels are at, or below, the detection level of *c.* 0.10 wt.%.

Calcite-rich carbonates have maximum MgO, MnO and FeO contents of 2.68%, 3.07% and 0.26% respectively, although concentrations are usually well below the maxima.

Epidotes (Fig. 7) are nearly pure epidote-clinozoisite solid solutions with the major trace elements MgO and MnO both present at levels of <0.25%. Those within the ore body have octahedral Al:Fe ratios of 1:2 and hence are pure Fe-end member epidotes. Those within the altered wall rocks show a slight shift towards clinozoisite.

Composition of the fluid phase

The volatile chemistry of apatites is a function of varying halogen and water fugacities within the volatile rich fluid from which they crystallize (Korzhinskiy, 1981). For the purpose of this paper, apatites are viewed as a solid solution between the three end members fluor-apatite (Fl-ap), chlor-apatite (Cl-ap) and hydroxy-apatite (OH-ap). As mixing between the three end members is essentially ideal (Tacker and Stormer, 1989), $a = X$ for each of the three end-members (where a = activity and X = mole fraction). The relationship between apatite chemistry and fluid chemistry can be simply defined such that, for the three apatite–fluid exchange reactions:

$$Ca_5(PO_4)_3F + H_2O = Ca_5(PO_4)_3OH + HF^o$$

$$Ca_5(PO_4)_3Cl + H_2O = Ca_5(PO_4)_3OH + HCl^o$$

$$Ca_5(PO_4)_3F + HCl^o = Ca_5(PO_4)_3Cl + HF^o$$

(where HF^o and HCl^o refer to the neutral aqueous species); and

$$K_D^{F-OH} = \frac{X_{HF} \cdot X_{OH-ap}}{X_{H_2O} \cdot X_{F-ap}}$$

$$K_D^{Cl-OH} = \frac{X_{HCl} \cdot X_{OH-ap}}{X_{H_2O} \cdot X_{Cl-ap}}$$

$$K_D^{F-Cl} = \frac{X_{HF} \cdot X_{Cl-ap}}{X_{HCl} \cdot X_{F-ap}}$$

where K_D is the relation between the molar fractions of the participating components in both solid and fluid phases (Korzhinskiy, 1981); and

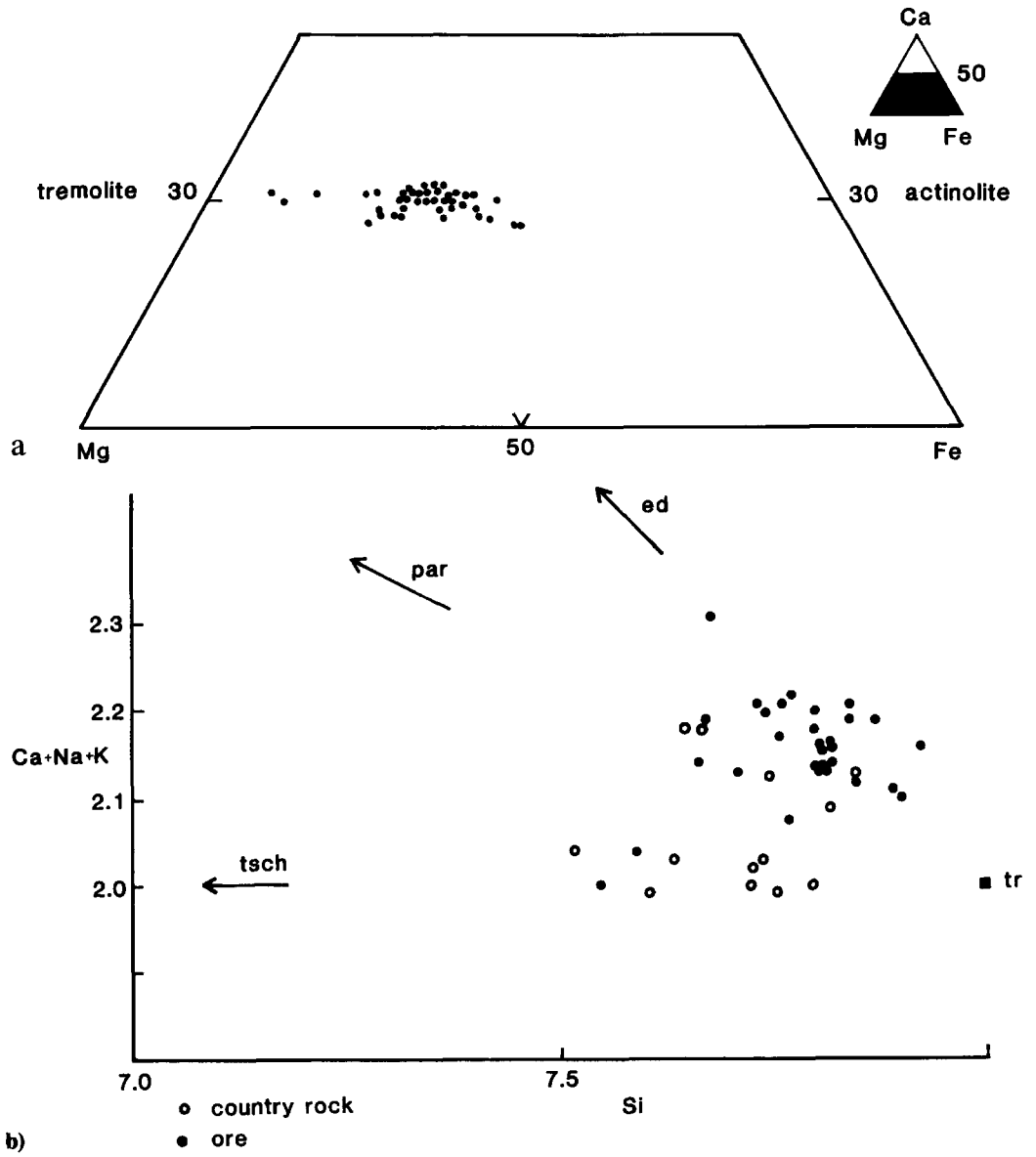

FIG. 6. Amphibole composition plots: (*a*) Ca-Fe-Mg. (*b*) Si *vs.* Ca + Na + K.

$$K_e^{F-OH} = \frac{f_{HF} \cdot a_{OH-ap}}{f_{H_2O} \cdot a_{F-ap}}$$

$$K_e^{Cl-OH} = \frac{f_{HCl} \cdot a_{OH-ap}}{f_{H_2O} \cdot a_{Cl-ap}}$$

$$K_e^{F-Cl} = \frac{f_{HF} \cdot a_{Cl-ap}}{f_{HCl} \cdot a_{F-ap}}$$

where K_e is the relation between the fugacites of H_2O, HCl and HF within the gas phase and the activities of the end member components within the solid phase (Korzhinskiy, 1981).

The experimentally derived data sets of Korzhinskiy (1981) and Zhu and Sverkensky (1991) provide values for K_D^{Cl-OH}, K_e^{Cl-OH}, K_e^{F-OH} and K_e^{F-Cl}. When combined with f_{H_2O} data (Burnham *et al.*, 1969) and using the methodology outlined by Yardley (1985), values of K_D and K_e can be used to

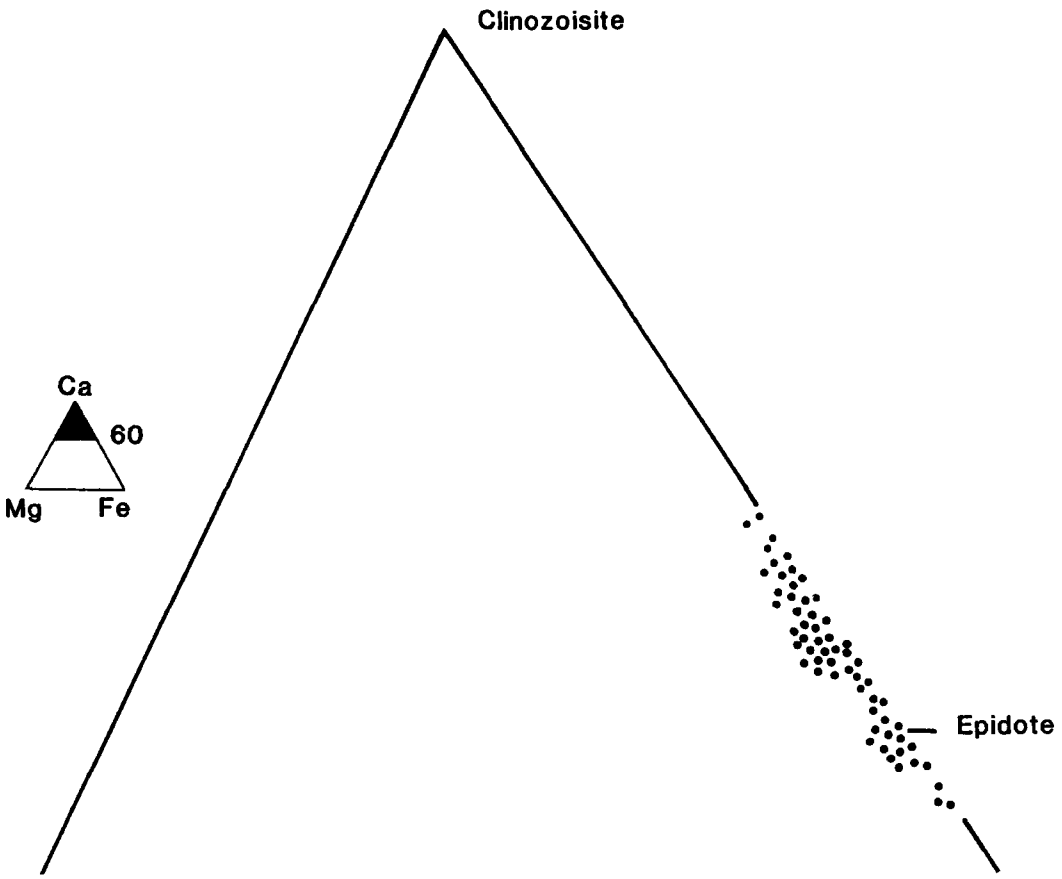

FIG. 7. Ca-Fe-Mg plot of epidote compositions.

calculate fugacity and mole fraction ratios between HF, HCl and H_2O within a hydrous fluid. The calculations summarized below are for a range of pressures and temperatures. Pressure estimates of 1 to 2 kbar have been derived for Jurassic to Cretaceous plutons emplaced into the Atacama Fault Zone (Grocott *et al.*, 1994) by use of the Al-in-hornblende geobarometer. On the basis of the amphibole type being actinolite-tremolite$_{ss}$ rather than hornblende, temperatures are estimated at 500 $\pm$ 50°C (cf. Liou *et al.*, 1974).

The results of the calculations are shown in Table 4. Variations in the halogen and water fugacities within a fluid permit the buffering of apatite chemistry through the apatite-fluid exchange equilibria. The tabulated results show the magnitude and trend of the changes in fluid chemistry that must have occurred through the evolution of the magnetite-apatite deposits in order to stabilize the significant zonations in apatite F and Cl contents analysed here. With the exception of values of X_{HCl}/X_{H_2O} near unity, derived from apatite cores from sample 1538, which have a high value of $X_{Cl\text{-}ap}$, all the calculated values of X_{HCl}/X_{H_2O}, f_{HCl}/f_{H_2O} and f_{HF}/f_{H_2O} are extremely low, implying that both HF and HCl were present only as minor components of an aqueous fluid. This is consistent with the experimental findings of Brenan (1993), which show that high values of $X_{F\text{-}ap}/X_{OH\text{-}ap}$ and $X_{Cl\text{-}ap}/X_{OH\text{-}ap}$ can be achieved at low HF and HCl contents in an aqueous fluid. Unfortunately, we have been unable to confirm the thermodynamically derived fluid compositions through direct measurement of entrapped fluids as many of the 'fluid inclusion' sites that we identified are now empty or contain merely residua of daughter, or captured, crystals.

Chlorine is volatile and thus partitions strongly into a magmatic vapour phase (Mathez, 1989*a*). By contrast, fluorine is far less volatile with low vapour-melt distribution coefficients. Candela (1989) lists vapour-melt distribution coefficients for Cl and F at 40 $\pm$ 10 and 0.2 $\pm$ 0.1 respectively. Candela (1989)

TABLE 4. Calculated values of X_{HCl}/X_{H_2O}, f_{HCl}, f_{HF} and f_{HCl}/f_{HF} in aqueous fluids in equilibrium with apatites in magnetite-apatite bearing ore. For method of calculation, see text. For sample 1538, apatite cores have $X_{Cl\text{-}ap}$ close to 1.0. To account for analytical errors in this sample, calculations have been done for values of $X_{Cl\text{-}ap}$ of 0.99 and 0.995. Where two sets of calculated fluid compositions are listed, as for sample 1134 core, these account for variations in apatite compositions

	X_{HCl}/X_{H_2O}	f_{HCl}	f_{HF}	f_{HCl}/f_{HF}
#1134				
core				
	0.0015–0.0020	0.55–2.15	0.50–3.21	0.62–1.13
	0.0004–0.0005	0.16–0.63	0.40–2.56	0.23–0.44
rim				
	0.0054–0.0076	2–8	0.04–0.26	28–54
	0.0014–0.0020	5–20	0.02–0.10	181–352
#1528				
core				
$X_{Cl\text{-}ap}$=0.99				
	1.078–1.503	403–1584	1.20–7.66	189–367
$X_{Cl\text{-}ap}$=0.995				
	2.156–3.007	806–3168	2.39–15.31	190–357
near rim				
	0.0117–0.0630	4–17	0.09–0.56	28–54
	0.0083–0.0116	3–12	0.13–0.84	13–54
rim				
	0.0091–0.0127	3–13	0.01–0.08	149–288
#1531: edge of zone				
core				
	0.0202–0.0281	8–30	0.50–3.22	8–16
near rim				
	0.0932–0.1300	34–137	0.05–0.30	423–818
rim				
	0.0139–0.0193	5–20	0.01–0.07	262–508
#1531: inner part of zone				
core				
	0.1087–0.1517	41–160	0.05–0.34	431–834
near rim				
	0.0278–0.0388	10–41	0.39–2.48	15–29
	0.0243–0.0339	9–36	0.43–2.76	12–23
rim				
	0.0165–0.0231	6–24	0.01–0.08	284–550

modelled fractionation of Cl and F into a vapour phase evolving from a magma. During decompression Cl will fractionate out of the magma into the vapour phase. The first fractionated vapours have the highest Cl contents. By contrast, F will increase within the residual magma, with only limited fractionation into the evolving vapour. For vapour evolved during crystallization, significant concentrations of F will only enter the vapour phase at a late stage of evolution. The vapour-melt distribution coefficient for Cl during crystallization is dependant on pressure of crystallization and water content within the evolving magma. At pressures appropriate to this study, of below 3–4 kbar, distribution coefficients are such that Cl will partition less strongly into the vapour phase than at higher pressures and water contents. Under these conditions, magmatic Cl contents will increase and vapour Cl contents increase with the latter reaching a maximum, late in the evolution history.

Candela (1986) applied a similar analysis to the partitioning of Cl and F into apatite crystallizing

within a felsic magma-vapour system. He demonstrated that, as a function of the systematic increase of F in both melt and vapour during crystallisation, $X_{F\text{-}ap}$ in apatites crystallized from the melt should increase from core to rim. At the pressures appropriate for this study, the Cl content of the melt will build, although at a lower rate than the F content. Hence $X_{F\text{-}ap}/X_{Cl\text{-}ap}$ will increase from core to rim, while both $X_{Cl\text{-}ap}$ and $X_{Cl\text{-}ap}/X_{OH\text{-}ap}$ will decrease. Within the apatites analysed here, no such consistent zonation is discernable. Some samples (e.g. 1528 and apatites from the zone centre of 1531) do show $X_{F\text{-}ap}/X_{Cl\text{-}ap}$ ratios increasing from core to rim, whereas others (i.e. 1134 and apatites from the zone margin of 1531) show the opposite trend. For sample 1531, textural evidence implies that acicular apatites in the zone margin, that grew perpendicular to the zone wall, grew before the spherical apatites found within the zone centre. The relative zonations shown by these apatites would be consistent with a model in which f_{HF} in the fluid initially decreased and then increased (*c.* 3.2 to *c.* 0.3 to *c.* 2.7; Table 4), with f_{HCl} behaving in the opposite manner (30 to *c.* 150 to 36). Increases in $X_{OH\text{-}ap}$ in the extreme rim regions of the analysed apatites would be consistent with late stage dilution of HF and HCl in an aqueous fluid.

These patterns may be caused by a number of factors. Firstly, Candela's (1986) apatite zonation scheme is modelled for apatites crystallising from a magma, and may not be directly applicable to apatites that crystallize from a magmatic vapour. Were the apatites to have crystallized from a magma, the crystallization of a F-bearing phase, such as amphibole or mica, would deplete magmatic F contents and invalidate the model. Secondly, the F and Cl contents of the evolving magma could have been modified by mixing with a new batch of unevolved magma. Thirdly, Candela's data (1986) suggest that, as F partitions strongly into the late stage magma and derived vapour, apatites that crystallize from this fluid should show a trend of increasing F content from core to rim. However, Brenan (1993) showed that, although values of $X_{Cl\text{-}ap}/X_{OH\text{-}ap}$ will continue to increase with increasing values of X_{H_2O}/X_{HCl} in the fluid, maximum levels of $X_{F\text{-}ap}/X_{OH\text{-}ap}$ will be attained at low contents of HF in an aqueous fluid, with levels of $X_{F\text{-}ap}/X_{OH\text{-}ap}$ decreasing with greater HF contents in the fluid. Thus, over-enrichment of F in the aqueous fluid, consistent with the late stages of a normal fractionation process, will not lead to an increase in $X_{F\text{-}ap}/X_{OH\text{-}ap}$, and could lead to a decrease in $X_{F\text{-}ap}/X_{Cl\text{-}ap}$. Brenan's experiments also show that, for any given content of HF or HCl in the aqueous fluid, the equilibrium values of $X_{F\text{-}ap}/X_{OH\text{-}ap}$ and $X_{Cl\text{-}ap}/X_{OH\text{-}ap}$ will be lower in a basic, Na-bearing aqueous fluid than in an acidic, Na-free one. The maximum values of $X_{F\text{-}ap}/X_{OH\text{-}ap}$ and $X_{Cl\text{-}ap}/X_{OH\text{-}ap}$ recorded here could not be attained in apatites in equilibrium with a basic fluid, but only in equilibrium with an acidic aqueous fluid. Brenan's experiments were conducted at temperatures (1050°C) considerably higher than those anticipated for this study, and caution should thus be used in applying them directly here.

Mathez (1989*b*) shows that F and Cl are partitioned in the apatite-magma-vapour system such that $(Cl/F)_{ap}<(Cl/F)_m<(Cl/F)_v$. He used this relationship to assert that, as the fractionation of chlorine from fluorine in a subsolidus vapour-apatite assemblage becomes extreme, chlorapatites should not form from a vapour. However, that chlorapatites do occur in the Fresia deposit suggests that apatite growth was not controlled simply through fractionations within a magma-vapour system. Mixing of a primary, magmatically-derived hydrothermal vapour phase with an aqueous fluid derived from the country rocks could modify f_{HF} and f_{HCl} levels in the fluid. In such a case, the decrease in $X_{F\text{-}ap}$ and increase in $X_{Cl\text{-}ap}$ and $X_{OH\text{-}ap}$ in rim regions would be consistent with dilution of f_{HF} in the magmatically-derived fluid by such mixing. The high Cl contents of the apatites, even in the rim regions, indicates that such a mixture was likely to be an H_2O–HCl fluid rather than a NaCl bearing one (cf. Brenan, 1993). Thus the apparent dichotomy of reduced $X_{F\text{-}ap}$ and increased $X_{Cl\text{-}ap}$ and $X_{OH\text{-}ap}$ can be resolved if the fluids that stabilized apatite growth represent dilution of an acidic, magmatic vapour derived from, or in equilibrium with, an Fe-rich magma, by mixing it with an HF-free, acidic, non-saline H_2O–HCl fluid with a low CO_2 content. This latter fluid could have been derived from the country rocks to the deposits.

Implications for apatite–magnetite ore genesis models

There has been considerable debate over whether Kiruna-type ores have a magmatic origin with the debate summarized by Hitzman *et al.* (1992), Nystrom and Henriquez (1994) and Bookstrom (1995). In terms of mineralogy and host rock lithologies, both the Fresia and Carmen deposits could be classified as Kiruna-type. Thus we need to consider whether they may be primary magmatic ores. There is considerable confusion as to what may define a magmatic deposit. Many of the features described for intrusive Fe-rich deposits (narrow dyke-like forms, incorporation of brecciated xenoliths of country rock, needle-like growths of amphibole and apatite perpendicular to vein walls or breccia fragment surfaces; see for instance, Geijer, 1967) may equally well fit hydrothermal deposits located within opening fractures, the early stages of

which are marked by hydrothermal brecciation. Guilbert and Park (1986) state that, throughout the Kiruna ore district, there is evidence for both magmatic and hydrothermal ores, with early high temperature ores being the product of magmatic segregation and later, lower temperature, ores having a hydrothermal origin. Magmatic deposits may (Nystrom and Henriquez, 1994) include *aa* and *pahoehoe* flow features, notably vesicular massive ore, lack of alteration in the host rocks, dyke-like feeder bodies, brecciation, columnar magnetite and dendritic magnetite, and pyroxene crystal forms indicative of rapid cooling and crystal growth. The first three characteristics represent the best evidence for magnetite flows and intrusions. However, Oreskes *et al.* (1994) show that many of the features displayed by the 'magmatic' El Laco deposit, may have formed from moderate temperature, hydrothermal fluids. Thus, there has to be a doubt as whether features described as being typically magmatic are indeed so, as opposed to being either a hydrothermal re-arrangment of magmatic features or a primary hydrothermal feature.

We have identified none of the first three features described by Nystrom and Henriquez (1994) at either Fresia or Carmen. The field evidence from the Fresia and Carmen deposits are indicative that a hydrothermal fluid was important in ore genesis. In support of this, we would cite the intense, greenschist-facies epidote and chlorite alteration of the host rocks; the thinness of some magnetite and epidote veinlets (Fig. 3c), which appears to indicate a low viscosity fluid; textures sugestive of conventional open-space hydrothermal precipitation; and the extreme size of some crystals which generally typifies a low viscosity hydrothermal or pegmatitic fluid. The presence of veinlets of epidote and magnetite, no more than a few mm in width, suggest the parent fluid to have had a low viscosity. On this analysis, the magnetite-apatite ores within the Atacama fault system most likely belong to the hydrothermal end of the magmatic-hydrothermal fluid spectrum. The fluid chemistries derived numerically from apatite chemistry are consistent with a conclusion that the deposits were derived from an evolved magmatic vapour mixed with formational aqueous fluids. The concentration of iron and the thermodynamics of the apatite-fluid equilibria (Brenan, 1993) suggest that the fluid mixture was both acidic and highly reduced.

Origin of the ore fluid

Guilbert and Park (1986) and Matthews *et al.* (1994) have discussed chemical controls that may influence the derivation of iron-rich melts, or vapours, by differentiation from a primary calc-alkaline magma. They infer that high Na contents, low oxygen fugacities and high phosphorus contents within the melt exert a control on the generation of Fe-rich melts and derived hydrothermal fluids.

By stabilizing Na-Fe-O complexes in the late stage melts, high sodium content in the melt may increase and flux the iron content of the melt. By analogy, Whitney *et al.* (1985) have shown that high iron contents can be stabilized in high-temperature, high-salinity aqueous fluids. In central Chile, none of the magmas are especially sodic. Jurassic and Cretaceous volcanics are locally spilitic, contain primary albite, and have a Na content of up to 6 wt.% Na_2O (Levi *et al.*, 1982; Rogers and Hawkesworth, 1989). The intrusive rocks that we have studied have Na contents of about 4 wt.% Na_2O and contain feldspars, none of which is more sodic than andesine in composition. As the effect of NaCl content in an aqueous fluid is to reduce F and Cl contents within apatites (Brenan 1993), and as magnetite-apatite ores are not commonplace in subduction zone environments, magmatic Na contents are not likely to be a critical control in their formation.

The presence of phosphorus in both the melt and the derived aqueous fluid is indicated by the presence of apatite within the magnetite-rich ores and of apatite inclusions within amphiboles within the Sierra Pastenes batholith. Matthews *et al.* (1994) have shown that, if a basic magma containing dissolved sulphide is mixed with a more oxidized silica-rich magma, the sulphides in the basic magma will be oxidized leading to a decrease in the magmatic Fe^{3+}/Fe^{2+} ratio. Low oxygen fugacities in the melt that result from this local reduction of Fe^{3+} will effectively restrict crystallization of magnetite at magmatic temperatures and allow a build up of iron in the residual fluids. The chemical reactions outlined in the magma mixing model of Mathews *et al.* (1994) demand that reduction of Fe^{3+} in the melt will lead to saturation of the melt in phosphorus with the resultant precipitation of apatite. If crystallization of apatite can be suppressed, this model gives the potential for an acidic, residual fluid rich in phosphorus and iron. The weakness of this model is that, although studies of granitoid bodies suggest magma mixing to be a common feature, not all of the iron-rich deposits within the Atacama Fault Zone carry apatite. Even if the evolution of Fe-rich magmas, and derived hydrothermal fluids, can be modelled readily, the localization of apatite-bearing Fe-rich deposits is a more intractable problem. Does this reflect a variation in phosphorus content within the magmas, such that the apatite-bearing magnetite deposits reflect hydrothermal fluids derived from primary, strongly reduced magmas with high phosphorus contents, and the apatite-free Fe-rich deposits reflect fluids derived from primary, strongly reduced magmas with low phosphorus contents?

An alternative, heterogeneous, source of phosphorus is indicated by present day upwelling of cold, deep oceanic waters in the vicinity of the Peru-Chile trench. This upwelling creates a patchy development of phosphorites on the trench-arc slope (Baturin 1982). The subduction-continental margin setting of western South America has been a feature since the Mesozoic. Thus it is possible to speculate that, in the Mesozoic, the patchy distribution of phosphorus on the trench-arc slope could have generated magmas with, locally, abnormally high phosphorus contents.

There is a further alternative to models by which the phosphorus content of the magma controls the stability of apatite. This is that the essential components of apatite can be scavenged by circulating acidic, reduced hydrothermal fluids from country rocks with a variable phosphorus content. In this context, Bell (1989) has demonstrated that the mid-Mesozoic sedimentary sequences of northern Chile contain evaporite sequences. Although these contain little phosphorus they are Cl-rich and circulating hydrothermal fluids would be likely to scavenge both Cl and Ca from them. Thus, it is possible that it is the presence of Ca that induces apatite precipitation from fluids that have a more or less constant level of dissolved phosphorus. When little Ca is available, massive magnetite ore will be generated with microscopic quantities of apatite, whereas when Ca is available, it will flux the phosphorus present resulting in localised concentrations of large apatite crystals. In such a case mixing of low-F high-Cl meteoric fluids with magmatically derived aqueous fluids would provide a mechanism for modifying f_{HF} and f_{HCl} levels in the mineralising fluids. Levi *et al.* (1982) indirectly provide support for this hypothesis. In studies of burial metamorphism of early Cretaceous basic flows from central Chile they showed that P was only partially mobile on the centimetre scale, whereas Ca was mobile on a scale larger than single flows and Na was pervasively passed to the flows from an external source. Unfortunately, Levi *et al.* (1982) provide no data relating to halogen mobility in the sequence.

Hence we would conclude that the Fe-P rich nature of the deposits is a function of magmatic differentiation (cf. Matthews *et al.*, 1994). The variable apatite concentration, and the nature of the halogen zonation profiles within the apatites is inconsistent with their crystallization directly from a volatile-rich, late-stage magma or its derived vapour. More likely, they represent the mixing of two distinct fluids: firstly, Fe-P-rich magmatic vapours derived by fractionation from primary magmas; and secondly, hydrothermal, meteoric fluids which have scavenged Ca and Cl from the country rock lavas. The implications of this are that: although the F may be magmatically derived, at least some of the Cl is scavenged from the country rocks; it may be possible to distinguish magmatic magnetite-apatite deposits from hydrothermal ones on grounds of mineral chemistry; and textures within magnetite-apatite deposits, that have previously been attributed purely to magmatic processes, may be the result of considerable hydrothermal reworking.

Acknowledgements

Fieldwork was funded by grants from the Royal Society and NERC. We acknowledge the support and assistance of the geologists and drivers of the SERNAGEOMIN, Santiago de Chile during field work. Mineral analyses were carried out at the Department of Earth Sciences in the University of Oxford with the assistance of Dr N.R. Charnley. Dr G. Watt of Oxford Brooks University provided BSE images and element maps. David Alderton, Kevin Blake and Andrew Rankin provided constructive reviews of the manuscript.

References

Atkin, B.P., Injque-Espinoza, J.L. and Harvey, P.K. (1985) In *Magmatism at a plate edge: the Peruvian Andes*. (W.S. Pitcher *et al.*, eds.) Blackie (Glasgow), pp. 261–70.

Baturin, G.N. (1982) *Developments in Sedimentology*, **33**. Elsevier (Amsterdam).

Bell, C.M. (1989) *Sedimentology*, **36**, 651–63.

Berg, K. and Baumann, A. (1985) *Earth. Planet. Sci. Lett.*, **75**, 101–15.

Blake, K.L. (1994) *Geological Society of America Annual meeting, Seattle, Abstracts with programs.* **26**, no 7, 380.

Bookstrom, A.A. (1977) *Econ. Geol.*, **72**, 1101–30.

Bookstrom, A.A. (1995) *Econ. Geol.*, **90**, 469–73.

Boric, R., Diaz, F. and Maksaev, M. (1991) *SENAGEOMIN Chile, Boletin* **40**, 246 pp.

Brenan, J.M. (1993) *Earth Planet. Sci. Lett.*, **117**, 251–63.

Brook, M., Pankhurst, R.J., Shepherd, T.J. and Spiro, B. (1987) *British Geological Survey, unpublished report.* 190 pp.

Brown, M. (1988) *V Congresso Geologico Chileno*, **III**, 153–66.

Brown M., Diaz F. and Grocott, J. (1993) *Geol. Soc. Amer. Bull.*, **105**, 1165–74.

Buchelt, M. and Cancino, C.T. (1988) In *The Southern Central Andes* (H. Bahlburg, C. Breitkreuz and P. Giese, eds). Lecture notes in Earth Sciences, Springer-Verlag, Berlin, **17**, 171–82.

Burnham, W., Holloway, J.R. and Davies, N.F. (1969) *Geol. Soc. Amer. Sp. Paper*, **132**, 96pp.

Candela, P.A. (1986) *Chem. Geol.*, **57**, 289–301.

Candela, P.A. (1989) *Rev. Econ. Geol.*, **4**, 203–21.

Clark, A.H., Farrar, E., Caelles, J.C., Haynes, S.J., Lortie, R.B., McBride, S.L., Quirt, G.S., Robertson, R.C.R. and Zentilli, M. (1976) *Geol. Assoc. Canada Sp. paper*, **14**, 23–59.

Cliff, R.A., Rickard, D. and Blake, K. (1990) *Econ. Geol.*, **85**, 1770–6.

Colley, H., Treloar, P.J. and Diaz, F. (1989) *Econ. Geol. Monograph*, **7**, 208–17.

Frietsch, R. (1978) *Econ. Geol*, **73**, 478–85.

Frutos, J. 1982. In *Ore genesis: the state of the art.* (G.C. Amstutz *et al.*, eds) *Soc. Geol. Appl. Min. Deposits. Spec. Publ.* **2**, 493–507. Springer-Verlag (Berlin).

Geijer, P. (1960) In *Archaean geology of Vasterbotten and Norrbotten, northern Sweden. Guide to excursions A32 and C26.* Sweden Geological Survey.

Geijer, P. (1967) *Sveriges Geologiska Undersokning. Ser C*, **624**, 32 pp.

Grocott, J., Brown, M., Dallmeyer, R.D., Taylor, G.K. and Treloar, P.J. (1994) *Geology*, **22**, 391–4.

Guilbert, J.M. and Park, C.F. (1986) *The Geology of Ore Deposits.* W.H. Freeman & Co. New York. 985 pp.

Henriquez, F., Dobbs, F., Espinoza, S., Nystrom, J., Travisany, V. and Vivallo, W. (1994) *7th Congreso geologica Chileno.* **2**, 822–4.

Hitzman, M.W., Oreskes, N. and Einaudi, M.T. (1992) *Precamb. Res.*, **58**, 241–87.

Korzhinskiy, M.A. (1981) *Geochem Internat*, **18**, 44–60.

Levi, B., Aguirre, L. and Nystrom, J.O. (1982) *Contrib. Mineral. Petrol.*, **80**, 49–58.

Liou, J.G.S., Kuniyoshi, S. and Ito, T. (1974) *Amer. J. Sci.*, **274**, 613–32.

Mathez, E.A. (1989*a*) *Rev. Econ. Geol.*, **4**, 21–31.

Mathez, E.A. (1989*b*) *Rev. Econ. Geol.*, **4**, 167–79.

Matthews, S.J., Jones, A.P. and Beard, A.D. (1994) *J. Geol. Soc. Lond.*, **151**, 815–23.

Naranjo, J.A. (1978) Carta 34. *Institute de Investigaciones Geologicas*, Santiago, Chile.

Nystrom, J.O. and Henriquez, F. (1994) *Econ. Geol.*, **89**, 820–39.

Oreskes, N., Rhodes, A.L., Rainville, K., Sheets, S., Espinoza, S. and Zentilli, M. (1994) *Geological Society of America Annual meeting, Seattle, Abstracts with programs.* **26**, no 7, 379.

Parak, T. (1975) *Econ. Geol.*, **70**, 1242–58.

Parak, T. (1984) *Econ. Geol.*, **79**, 1945–9.

Park, C.F. (1961) *Econ. Geol.*, **56**, 431–6.

Park, C.F. (1972) *Econ. Geol.*, **67**, 339–49.

Pichowiak, S. (1993) In *Tectonics of the South Central Andes: structure and evolution of an active continental margin.* (K-J. Reutter, E. Scheuber and P.J. Wigger, eds) Springer-Verlag, Berlin. Pp. 203–17.

Potts, P.J. and Tindle, A.G. (1989) *Mineral. Mag.*, **53**, 357–62.

Ramsay, J.G. and Huber, M,I. (1983) *The techniques of modern structural geology. Volume 1. Strain analysis.* Academic Press. 307 pp.

Rogers, G. and Hawkesworth, C.J. (1989) *Earth Planet. Sci. Lett.*, **91**, 271–85.

Romer, R.L., Martinsson, O. and Perdahl, J.A. (1994) *Econ. Geol.*, **89**, 1249–61.

Scheuber, E. and Andriessen, P.A.M. (1990) *J. Struct. Geol.*, **12**, 243–57.

Sibson, R.H. (1977) *J. Geol. Soc. Lond.*, **133**, 191–214.

Sillitoe, R.H. (1976) *Geol. Assoc. Canada. Sp. paper*, **14**, 59–100.

Tacker, R.C. and Stormer, J.C. (1989) *Amer. Mineral.*, **74**, 877–88.

Travisany, V., Henriquez, F. and Nystrom, J.O. (1995) *Econ. Geol.*, **90**, 438–44.

Vidal, C.E. (1985) In *Magmatism at a plate edge: the Peruvian Andes.* (W.S. Pitcher *et al.*, eds). Blackie (Glasgow) Pp. 243–9.

Whitney, J.A., Hemley, J.J. and Simon, F.O. (1985) *Econ. Geol.*, **80**, 444–60.

Yardley, B.W.D. (1985) *Mineral. Mag.*, **49**, 77–80.

Zhu, C. and Sverjensky, D.A. (1991) *Geochim. Cosmochim. Acta*, **55**, 1837–58.

[*Manuscript accepted 20 October 1995*]